An Analysis of the 70-Meter Antenna Hydrostatic Bearing by Means of Computer Simulation

R. D. Bartos

Ground Antennas and Facilities Engineering Section

Recently the computer program "A Computer Solution for Hydrostatic Bearings with Variable Film Thickness," used to design the hydrostatic bearing of the 70-meter antennas, was modified to improve the accuracy with which the program predicts the film height profile and oil pressure distribution between the hydrostatic bearing pad and the runner. This article presents a description of the modified computer program, the theory upon which the computer program computations are based, computer simulation results, and a discussion of the computer simulation results.

I. Introduction

A significant level of engineering effort was expended in the early 1960s to develop a design for the hydrostatic bearing to support the alidade structure of the 64-meter DSN antennas. The hydrostatic bearing was designed using a computer program entitled "A Computer Solution for Hydrostatic Bearings with Variable Film Thickness," written by Dr. Vittorio Castelli while employed at the Franklin Institute. Until 1992 this program was used to estimate the oil film height that could be expected between the bearing pad and the runner under various operating conditions and did not consider pedestal deflections, pad deflections, or imperfections in the flatness of the runner when making oil film height predictions. Because the computer program did not consider the deflection and flatness issues, JPL engineering has not had complete confidence in the program's ability to accurately predict the oil film height of the hydrostatic bearing. In an effort to improve JPL's capability to accurately estimate the hydrostatic bearing oil film height, JPL contracted Dr. Castelli to modify the original computer program. The modified program allows

JPL to assess the effects of oil flow through the recesses, oil temperature, pedestal deflection, pad deflection, runner flatness, and pad loading. The additional program capabilities were determined to be necessary so that JPL can accurately assess the effects of adding additional weight to the antenna bearings as was done in 1987 when the 64-meter antennas were upgraded to 70-meter antennas. This article outlines the capabilities of the modified hydrostatic bearing program and presents the results of the program under various operating conditions of the hydrostatic bearing.

II. Hydrostatic Bearing Theoretical Model

The hydrostatic bearing of the DSN 70-meter antennas consists of a rectangular steel bearing pad connected to the antenna alidade frame by a self-aligning spherical joint. The pad rests on a relatively flat steel runner that is attached to the antenna pedestal. The bearing functions by pumping oil at a constant flow rate into each of six recesses located on the bottom of the pad so that the

antenna floats on a thin oil film as the oil flows out of the recess between the pad and the runner. The computer program developed by Dr. Castelli predicts the film height profile and pressure distribution between the bearing pad and the runner by finding, through an iterative process, the film height profile and pressure distribution that satisfy a set of governing equations. The governing equations are presented in this section.

A. Oil Film

The equation which governs the pressure distribution and oil film height between the pad and the runner is the Reynolds equation. The Reynolds equation is given by the expression[1]

$$\frac{\delta}{\delta x}\left(ph^3\frac{\delta p}{\delta x}\right) + \frac{\delta}{\delta y}\left(ph^3\frac{\delta p}{\delta y}\right) = 0 \qquad (1)$$

where p is the pressure, h is the film height, and x and y are Cartesian coordinates (see Appendix for glossary). The program assumes that oil is provided to each of six recesses at a constant flow rate and oil viscosity. The oil from the recesses flows in the clearance between the pad and the runner back to the reservoir. The behavior of the oil flow through the clearance between the bearing pad and the runner is governed by the equations [1]

$$q_x = -\frac{h^3\delta y}{12\mu}\left(\frac{\delta p}{\delta x}\right) \qquad (2)$$

and

$$q_y = -\frac{h^3\delta x}{12\mu}\left(\frac{\delta p}{\delta y}\right) \qquad (3)$$

where μ is the absolute viscosity of the oil, q_x is the flow rate in the x-direction at a point beneath the pad through a slot of height h and width δy, and q_y is the flow rate in the y-direction at a point beneath the pad through a slot of height h and width δx. The kinematic viscosity of the oil is determined for a particular oil using Walther's Equation given by[2]

$$\log\left(\log\left(\nu + a\right)\right) = m\log\left(T\right) + b \qquad (4)$$

where ν is the kinematic viscosity in centistokes, a is a constant equal to 0.6 centistokes, T is the absolute temperature, and m and b are constants of a particular oil. The constants m and b for an oil are determined by measuring the viscosity of the oil at two different temperatures and solving the two equations derived from Eq. (4) simultaneously for m and b. The absolute viscosity used in Eqs. (2) and (3) is found through the relationship [1]

$$\mu = \rho\nu \qquad (5)$$

where ρ is the oil density. The computer program written by Dr. Castelli requires that the absolute viscosity be input at two different temperatures and assumes that the oil density is constant at 900 kg/m^3 such that Eqs. (4) and (5) can be used to compute the absolute viscosity at any operating temperature.

The alidade structure is supported by the hydrostatic bearing in a state of static equilibrium; that is, the acceleration of the bearing pads is zero in the vertical direction. Hence the load supported by the bearing must be equal to the pressure forces under the pad. The total load supported by the pad is related to the pressure forces under the pad through the equation[3]

$$W = \int\int p\,\delta x\,\delta y \qquad (6)$$

where the integrations are taken over the area on the bottom of the bearing pad. Since the bearing pad is mounted on a spherical grease-lubricated joint, the total moments acting on the pad as produced by the pressure forces must be zero. The moments acting on the pad about the x- and y-axes are computed using the equations[4]

$$W_x = \int\int py\,\delta x\,\delta y \qquad (7)$$

and

$$W_y = \int\int px\,\delta x\,\delta y \qquad (8)$$

respectively, where the integrations are taken over the area on the bottom of the bearing pad.

Equations (2) through (8) provide a set of constraint equations for the Reynolds equation which governs the

---

[1] Vittorio Castelli, *Report on the Development of a Computer Program for the Simulation of the Hydrostatic Bearing Problem of the 70 Meter Antenna Systems*, JPL D-10449 (internal document), Jet Propulsion Laboratory, Pasadena, California, p. 3, June 1992.

[2] Ibid., p. 18.

[3] Ibid., p. 3.

[4] Ibid., pp. 3–4.

pressure distribution and oil film height between the pad and the runner.

B. Deflection of the Pedestal and Pad

The deflections of the antenna pedestal and the bearing pad are computed by the modified hydrostatic bearing program using a numerical Green's function method. The use of the Green's function method to simulate the deflection of the pedestal and the pad is advantageous because it allows the deflection problem to be solved once using finite-element analysis for a given set of loading conditions. The solution for a given set of loading conditions can subsequently be scaled within the hydrostatic bearing program for other loading conditions with significantly less computation and without coupling a finite-element analysis to the hydrostatic bearing program. A Green's function gives the deflection of a structure at a point B on the structure resulting from a unit load applied at point A on the structure. Because Green's functions are based on linear elastic theory, the deflection of a point B due to a load K times the unit load applied at point A will be K times the deflection that exists with the unit load. In addition, the total deflection at point B will be the summation of the deflections at point B from the loads applied at all other points on the structure. The Green's functions for the various loading and deflection points were computed by Ed Solcz using the ALGOR finite-element analysis package for the DSS-14 pad and pedestal.[5] Although the basic principles upon which a Green's function is based are the same when analyzing either the pedestal or pad deflection, the way in which a Green's function is implemented within the computer program is slightly different as described below.

1. Pedestal Deflection. The Green's functions describing the deflection of the pedestal have the form[6]

$$G(r_L, r_d, \theta_d, E, \nu) = \text{the deflection at point B as the}$$
$$\text{result of a unit load at point A} \quad (9)$$

where E is the modulus of elasticity of the pedestal material, ν is Poisson's ratio, and r_L, r_d, and θ_d are geometrical dimensions as defined in Fig. 1. As a result of the symmetry of the antenna pedestal, the Green's functions were computed for unit loads applied to different radii on the bearing runner. The pedestal deflection at a coordinate (x, y) beneath the bearing pad is computed using the equation[7]

[5] Ibid., pp. 65–87.

[6] Ibid., p. 8.

[7] Ibid., pp. 8–9.

$$e(x, y) = \int \int p(\xi, \eta) G(r_L(\xi, \eta), r_d(x, y),$$

$$\theta_d(x, y), E, \nu) \delta\xi \, \delta\eta \quad (10)$$

where the integrations are taken over the area on the bottom of the bearing pad.

2. Pad Deflection. The pad deflection is computed using the equation[8]

$$g(x, y) = P_{avg} d_u(x, y) + P_o d_o(x, y) + P_o^* d_o^*(x, y) \quad (11)$$

where

$$P_{avg} = \frac{1}{6}(P_1 + P_2 + P_3 + P_4 + P_5 + P_6) \quad (12)$$

$$P_o = \frac{1}{2}(P_1 + P_6 - P_2 - P_5) \quad (13)$$

$$P_o^* = \frac{1}{2}(P_3 + P_4 - P_2 - P_5) \quad (14)$$

and where $d_u(x, y)$ is the Green's function describing the deflection of the pad due to a uniform pressure distribution beneath the pad of unit magnitude, $d_o(x, y)$ is the Green's function describing the pad deflection when uniform pressure distributions of unit magnitude are present in areas 1 and 6 according to Fig. 2, $d_o^*(x, y)$ is the Green's function when uniform pressure distributions of unit magnitude are present in areas 3 and 4 according to Fig. 2, and P_i is the average pressure over area number i according to Fig. 2.

C. Oil Film Height Profile

Once the pedestal and pad deflections have been determined, the oil film height profile between the pad and the runner is computed using the equation[9]

$$h(x, y) = h(0, 0) + \phi_x y + \phi_y x + [e(x, y) - e(0, 0)]$$
$$+ [g(x, y) - g(0, 0)] + [b(x, y) - b(0, 0)] \quad (15)$$

where

[8] Ibid., pp. 9–10.

[9] Ibid., p. 4.

$h(x, y)$ = oil film height

$e(x, y)$ = absolute deflection distribution of the pedestal positive up

$g(x, y)$ = deflection distribution of the pad positive up

$b(x, y)$ = distribution of the bump on the runner positive up

ϕ_x = tilt angle of the pad about the x-axis in radians

ϕ_y = tilt angle of the pad about the y-axis in radians

The computer program arrives at the final film height profile through an iterative process that converges on the final solution where all of the governing equations presented in Eqs. (1) through (15) are simultaneously satisfied.

D. Pump Flow Curves

One of the limitations of the modified hydrostatic bearing program developed by Dr. Castelli is that the program assumes that oil is provided to the bearing recess at a constant specified flow rate. However, in practice, this is not the case because the De Laval Turbine, Inc., IMO B12-LBSX-118 pumps which are used to supply oil flow to the bearing recesses actually provide a flow rate according to the equation

$$Q = 0.4S - 466.823\sqrt{\frac{\Delta p}{\nu}} \text{ ml/sec} \qquad (16)$$

where S is the pump speed in rpm, Δp is the differential pressure across the pump in MPa, and ν is the kinematic viscosity in centistokes. Figure 3 shows how the output flow of the pump varies with oil kinematic viscosity and differential pressure across the pump using Eq. (16). The curves shown in Fig. 3 should distort downward as a pump wears because the coefficient 466.823 is expected to increase in magnitude as the internal pump clearances become larger.

III. Computer Program
A. Description

The original computer program used to analyze the hydrostatic bearing was modified by Dr. Castelli to expand the program's capabilities. The modified program allows the user to input a wide variety of parameters related to

the operation of the hydrostatic bearing. This provides JPL with a great deal of flexibility in simulating the hydrostatic bearing under many operating conditions. The computer program allows the program user to specify the geometry of the bearing pad, input a constant oil flow rate to each recess, input the viscosity-to-temperature relationship of the oil, specify the operating temperature of the oil, input the load acting on the pad, input the resultant moments acting on the pad, input the Green's functions for the pedestal and pad deflections, input the modulus of elasticity of the pedestal and pad material, and input a runner profile to simulate imperfections in the flatness of the runner surface. Once provided with all of the required inputs, the computer program computes the film height profile, pressure distribution, recess pressures, and minimum film height through an iterative process.

B. Computer Simulation

Several computer simulation runs were made in order to determine the sensitivity of the hydrostatic bearing to various parameters. A Lahey Compiler was used to process all of the Fortran 77 source code, and the program was run using a 386 microprocessor. An average of 30 min of computation time was required to provide results. This section presents the results of the hydrostatic bearing analysis performed using the modified hydrostatic bearing computer program.

1. **Simulation Conditions.** Due to the large number of input parameters which influence film height, it would not be feasible to run the hydrostatic bearing program for every possible operating condition. To keep the amount of computer output and computation time to a minimum while still obtaining useful information, a small number of computer runs were made to determine how sensitive the hydrostatic bearing performance is to changes in the input parameter values. This was accomplished by running the simulation program using parameter values that are higher and lower than the value believed to currently exist under normal operation at DSS 14. The largest pad load at DSS 14 is believed to be approximately 1.3×10^7 newtons.[10] The geometry of the bearing pad used to support the DSN 70-meter antennas is shown in Fig. 4. ISO 150 oil was supplied to each of the six recesses at a temperature of 308 K. The flow rate was assumed to be a constant flow rate of 550 ml/sec to each recess. This flow rate was selected for simulation purposes because the value is conservative since the flow is not expected to be less

[10] B. Saldua, *Baseline of DSS-14 Hydrostatic Pad Loads*, JPL Interoffice Memorandum 3323-92-001 (internal document), Jet Propulsion Laboratory, Pasadena, California, January 2, 1992.

than this with an unworn pump based upon expected recess pressures, oil temperature estimates, and the pump performance curves shown in Fig. 3. Unless specified in the results, all computer runs were made using the runner profile shown in Fig. 5. The data presented in Fig. 5 are based upon actual sensor data collected on October 16, 1992, and the profile calculation was made according to the currently authorized DSN method.[11] The locations of the sensors used to obtain the runner profile are shown in Fig. 4.

2. Oil Temperature. The temperature of the oil supplied to the recesses of the hydrostatic bearing has a major effect on the performance of the bearing. The performance of the bearing is affected by oil temperature because the oil properties change with temperature. Figures 6, 7, and 8 show how the oil properties of absolute viscosity, kinematic viscosity, and density vary with oil temperature for ISO 150 oil and ISO 220 oil. A graph of the minimum film height as a function of oil temperature for ISO 150 oil and ISO 220 oil is shown in Fig. 9. Figures 10 and 11 show the recess pressures as a function of oil temperature for ISO 150 oil and ISO 220 oil, respectively. Currently all of the 70-meter antennas operate the hydrostatic bearing using ISO 150 oil. The behavior curves for ISO 220 oil have also been included because some individuals have suggested improving film height by using a more viscous oil. A complete discussion of the benefits and problems of using a more viscous oil in the hydrostatic bearing is provided later in this article.

3. Recess Flow. The oil flow rate provided to a particular recess is dependent upon the oil viscosity and differential pump pressure as depicted in Fig. 3. The flow rate provided by a pump is also related to the degree of pump wear. Therefore, the sensitivity of the bearing performance to oil flow rate through the recess is of significant interest. Figure 12 shows the film height as a function of oil flow through the recess assuming all recesses receive the same flow. The recess pressures are shown as a function of oil flow rate in Fig. 13. Because the pumps operate at different pressures and are worn to different degrees, it is unlikely that every pump provides exactly the same flow rate. To determine what effect this would have on the performance of the hydrostatic bearing, several runs were performed while providing different oil flow rates to each of the recesses. The results of these runs are presented in Table 1.

[11] W. Kuehn, *Software Definition Document for Hydrostatic Bearing Instrumentation*, SDD-DOA-5534-SP (internal document), Jet Propulsion Laboratory, Pasadena, California, pp. 10–12, March 8, 1984.

4. Load. Modifications to the 70-meter antennas are frequently made in order to improve their capabilities. These modifications generally require additional weight to be added to the alidade structure, which increases the load that must be supported by the hydrostatic bearing. Therefore there is a great deal of interest at JPL in determining the performance effects of altering the load supported by the hydrostatic bearing. Figures 14 and 15 show the minimum film height and recess pressures, respectively, as a function of pad load.

5. Pedestal and Pad Deflections. The hydrostatic bearing program originally developed in the early 1960s did not take into consideration the deflection of the pedestal and the pad when predicting the film height and pressure distributions. Hence, the effect of deflection on hydrostatic bearing performance has been unknown and of great concern to JPL for many years. In order to identify the effects of pedestal and pad deflections, four computer runs were made while assuming a flat runner profile. The four computer runs consisted of one run where the pedestal and the pad were infinitely stiff, one run where the pad deflected and the pedestal was infinitely stiff, one run where the pad was infinitely stiff and the pedestal deflected, and one run where both the pedestal and the pad deflected. The minimum film height and recess pressures for each of these runs are presented in Table 2; graphs of the film height profiles for these cases are shown in Figs. 16 through 23.

6. Runner Profile. DSN operations have expended a large degree of effort to shim the runner to a flat surface in order to avoid low film height alarms. As a result of the large quantity of resources used to perform the shimming operations, JPL is interested in determining the effects that imperfections in runner flatness have upon the hydrostatic bearing performance. Table 3 shows the minimum clearance and recess pressure that arise when the hydrostatic bearing is operated with a perfectly flat runner and when it is operated with the DSS-14 runner profile shown in Fig. 5. The graphs of the clearance profiles with a flat runner surface and with the DSS-14 runner profile are shown in Figs. 22 through 25.

IV. Discussion of Computer Program Results

This section presents a discussion of the results gathered from the computer analysis.

A. Oil Temperature

An examination of the relationship between oil temperature and hydrostatic bearing film height shown in Fig. 9

reveals that the oil temperature and the type of oil used in the hydrostatic bearing have a significant effect on the minimum film height present between the bearing pad and the runner. Currently the hydrostatic bearing instrumentation group provides a low film height warning when the clearance between the pad and the runner is less than 127 μm (0.005 in.) and sets the antenna brake when the clearance is less than 76.2 μm (0.003 in.) while the antenna is moving. DSS 14 currently operates the hydrostatic bearing using ISO 150 oil at a temperature of approximately 308 K (94.73 deg F). At this oil temperature and under DSS-14 operating conditions the minimum film height is expected to be approximately 151.6 μm (0.00597 in.). Hence DSS 14 has approximately a 24.6-μm (0.00097-in.) margin of safety against a warning. This is not very much when one considers the uncertainty in the operating conditions of the bearing. It is clear from Fig. 9 that the minimum film height could be significantly increased by operating the hydrostatic bearing at a lower temperature or using ISO 220 oil instead of ISO 150 oil in the bearing. In practice there may be some difficulty in lowering the oil temperature to a desired level to obtain better film heights because lowering the oil temperature decreases the differential temperature between the bearing oil and the cooling water. This, in turn, decreases the rate at which heat can be removed from the oil through the heat exchanger. If the heat exchanger cannot remove the heat generated in the system at a desired oil temperature, the heat exchanger cannot supply oil at that desired temperature. To obtain better film heights without having this difficulty, ISO 220 oil could be used instead of ISO 150 oil. However, this method of improving oil film height may create problems also because the temperature at which the pumps have enough horsepower to perform a cold start during the winter months is increased and because the seals in the high pressure pumps can be damaged during a cold start if the viscosity of the oil passing through the pump is greater than 630 centistokes. Modifications to the existing system may be required to implement either of these methods of improving hydrostatic bearing film height. The identification of any required modifications requires additional study.

Figures 10 and 11 show that the recess pressures do not change significantly as the temperature of the oil changes.

B. Recess Flow

The results of the computer analysis performed to determine the sensitivity of the minimum bearing film height to the recess flow rate shown in Fig. 12 indicate that the flow rate has a moderate effect on the oil film height. The effect of recess flow is considered moderate because relatively large changes in flow rate are required to affect the minimum film height by an amount that is considered significant. Although the effect of oil flow is moderate, it should not be ignored, because large variations can occur since pump flow rates can vary by large amounts as the result of variations in oil viscosity and differential pressure across the high pressure pumps, as indicated in Fig. 5. Pump wear will also cause variations in flow rate because clearances are increased within the pump. The extent to which pump wear affects the output flow rate of the high pressure pumps is not known because instrumentation to measure the output flow rate of the pumps while under load does not currently exist.

Based upon Fig. 12, it would be logical to consider improving the bearing film height by increasing the flow rate provided to each recess. However, this is not a cost-effective method of improving film height for the following reasons:

(1) All 18 high pressure pumps and the electric motors which drive the pumps would have to be replaced in order to provide the increased flow rate.

(2) Increased electric power consumption would be required to drive the pumps since the output pressure of the pumps would not change with an increase in flow, as indicated by Fig. 13.

(3) The precharge pumping system would have to be completely redesigned to accommodate the higher flow rates and to provide an oil cooling system capable of dissipating the additional thermal energy generated by the system.

C. Load

Occasionally it is desirable to add additional equipment to the antenna in order to improve its performance. The addition of equipment adds to the weight which must be supported by the hydrostatic bearing. Figure 14 shows the extent to which the minimum film height decreases with an increase in the load supported by the bearing. This graph can be used to estimate the decrease in film height resulting from any future additional weight to the antenna in order to determine if the additional weight could result in low film height alarms. An increase in bearing pad load also results in an increase in recess pressures, as shown in Fig. 15. The pumps used on the 70-meter antenna are capable of operating at pressures up to 27.58 MPa. When a proposal is made to add weight to the antenna, an estimate of the high pressure pump output pressure should be made using Fig. 15 to determine if the maximum pump operating pressure is exceeded and if the electric motors are capable of providing the additional power to rotate the pumps. Since additional weight results in an increase in

pump pressure, an increase in antenna weight also results in an increase in the thermal energy generated by the system. The cooling system must be checked to ensure that it is capable of dissipating the additional thermal energy from the oil at the desired operating temperature or low film height alarms may occur due to the inability of the system to maintain the correct oil temperature. The increase in pump pressure resulting from increased pad load also results in a reduced output flow from the pumps as indicated in Fig. 3. The effects of the reduction in pump flow are expected to be moderate for the reasons stated in Section IV.B but should be considered when planning increases in pad loading.

It is important to realize that Fig. 15 can be used to make rough estimates of antenna pad loads. Pad load estimates can be made by measuring the pump output pressures at the stations and using Fig. 15 to correlate the pump pressures to the pad load.

D. Pedestal and Pad Deflection

The design of the hydrostatic bearing in the 1960s was based upon the original computer program "A Computer Solution for Hydrostatic Bearings with Variable Film Thickness." This program did not consider pad or pedestal deflections when making film height profile or pressure distribution predictions. The designers of the hydrostatic bearing attempted to remove the effect of pedestal and pad deflections by trying to design the pedestal and pad such that the deflections of the pedestal and pad would be matched. By matching the pedestal and pad deflections the bearing designers hoped to obtain a uniform film height beneath the pad as would be the case if the pedestal and pad did not deflect at all.[12] The modified computer program assesses the effects of both pedestal and pad deflections. An examination of the computer simulation results from the modified program shown in Table 2 and Figs. 16 through 23 reveal that the deflections of the pedestal and the pad cause the minimum film height to be significantly lower than was expected when the hydrostatic bearing was designed without consideration of the pad and pedestal deflections. Table 2 and Figs. 16, 17, 22, and 23 show that the expected minimum film height decreases by 114.6 μm (0.0045 in.) when both pedestal and pad deflections are considered compared to when no deflections are considered as was the case when the hydrostatic bearing was designed. Hence, the deflection of both the pedestal and the pad are

believed to contribute significantly to the low film height problems experienced by the 70-meter antennas.

E. Runner Profile

Operations personnel have expended a great deal of effort over the years in order to shim beneath the hydrostatic bearing runner in order to obtain a "flat" runner so that low film height alarms do not occur. The shimming is necessary to keep the runner flat because corrosion of the runner, corrosion of the sole plates, and degradation of the grout cause the runner profile to change over time. To assess the effects of a nonflat runner, a comparison of the minimum film height and recess pressures was made between a computer simulation performed with a flat runner and a simulation performed with the DSS-14 runner profile shown in Fig. 5. The results of the comparison provided in Table 3 show that there is a 7.08-μm (0.0003-in.) decrease in minimum film height when the DSS-14 profile is used. This decrease in minimum film height due to the imperfect DSS-14 runner is not considered to be significant. The fact that the DSS-14 runner profile did not produce a significant degradation in film height does not indicate that the runner profile does not have a significant effect on bearing performance but rather that the DSS-14 profile used for the computer simulations does not have a significant effect. In practice operations personnel have found that the runner profile has a large effect on film height. Further investigation is required to identify the kinds of runner profiles that cause film height problems.

F. Recess Pressure Variations

Field measurements of the recess pressures at DSS 14 show a variation among the pressures of different recesses. Measurements taken from pad 3 on December 10, 1991, revealed the pressures of recesses 1 through 6 as defined in Fig. 4 to be 9.65 MPa, 10.34 MPa, 7.58 MPa, 8.62 MPa, 9.65 MPa, and 11.38 MPa, respectively.[13] The difference between the highest and lowest pressure is 3.8 MPa. This variation in recess pressures is much larger than the variations of the recess pressures predicted by the computer simulations as shown in Figs. 10, 11, 13, and 15, and Tables 1 through 3. An examination of Table 2 shows that some variations among recess pressures result from the deflection of the pad and runner. Table 3 shows that variations in recess pressures can be caused by the runner profile. Although the deflections of the pad and pedestal and the runner profile result in some variation of the recess pressures, neither produced a variation as high as the one observed in practice. Several computer simulations were performed with different flow rates to the recesses to see if

[12] The NASA/JPL 64-Meter-Diameter Antenna at Goldstone, California: Project Report, Technical Memorandum 33-671 (internal document), Jet Propulsion Laboratory, Pasadena, California, pp. 63–65, July 15, 1974.

[13] B. Saluda, op. cit.

the large variations in recess pressures could be attributed to variations in pump flow rate. The results of these simulations presented in Table 1 indicate that only small variations in recess pressures can occur from differences in the flow rates provided to each recess. Further investigation is required to determine the reasons for the variations among the recess pressures observed on the 70-meter antennas.

G. Measurement of the Runner Profile and Bearing Film Heights

The effects of the runner profile on bearing performance were assessed using a runner profile computed according to the method currently approved by the DSN[14] from measurements taken at DSS 14 with the hydrostatic bearing instrumentation group. The results of the computer simulations presented in this article and discussions with station personnel at DSS 14 bring in to question the accuracy to which this runner profile is known with respect to a plane perpendicular to the gravity vector. If the runner profile cannot be determined accurately then it is difficult to try to assess the actual effects of the runner profile on the bearing film height.

The runner profile is currently measured using the hydrostatic bearing instrumentation group. This instrumentation group consists of five linear variable displacement transducer (LVDT) sensors mounted to a bar which is attached to one edge of bearing pad 3 as shown in Fig. 4. Two tipping probes, probes 6 and 7, are mounted over the pad to measure the motion of the top of the pad relative to the alidade frame. Probe 6 measures the vertical motion of the pad directly over probe 1 while probe 7 measures the vertical motion of the pad directly over probe 5. The vertical motion of the alidade frame relative to the azimuth bull gear is measured using LVDT probe number 9, mounted to the alidade frame with the tip of the probe riding on the top of the bull gear. The profile of the bull gear is determined by using a 10-degree level bar which determines the difference in elevation with respect to gravity of points at 10-degree intervals along the bull gear as shown in Fig. 26. The differences are added together to obtain the profile of the bull gear with respect to any measurement point defined to be zero on the bull gear. The profile of the bull gear between the 10-degree measurement points is interpolated using a 3-1/3-degree level bar mounted to the alidade frame that has three LVDT probes, probes 9, 15, and 16, mounted on it 3-1/3 degrees apart with respect to the antenna center. The bull gear probe previously mentioned is the center probe on this level bar. A diagram showing the

location of all the probes is shown in Figs. 27 and 28. It is clear from Fig. 27 that

$$Z + G + Y = X + T + h \tag{17}$$

Differentiating Eq. (17) yields

$$dZ + dG + dY = dX + dT + dh \tag{18}$$

Rearranging Eq. (18) produces an equation for the differential change in runner profile given by

$$dZ = dX + dT + dh - dG - dY \tag{19}$$

where dh is the change in film height as measured by probes 1 through 5, dT is the change in distance between probes 1 through 5 and the line extended between the pad contact points of probes 6 and 7, dX is the change in elevation between the top of the bearing pad and the alidade frame, dY is the change in elevation between the alidade frame and the bull gear measured using probe 9, and dG is the change in the bull gear profile as measured by the 10-degree level bar and interpolated using probes 9, 15, and 16. The value of dT is assumed to be zero by the current measurement scheme. The profile of the runner is determined by computing the change in runner height from the location on the runner that is defined as having zero runner height with respect to a plane perpendicular to gravity. The equation used to compute the runner profile under probes 1 through 5 at a particular azimuth angle is[15]

$$Z_i = P_9 + G - P_i - \frac{P_6 + P_7}{2} - \left(\frac{P_6 - P_7}{2}\right) a_i \tag{20}$$

$$a_1 = 1.0 \tag{21}$$

$$a_2 = 0.5 \tag{22}$$

$$a_3 = 0 \tag{23}$$

$$a_4 = -0.5 \tag{24}$$

$$a_5 = -1.0 \tag{25}$$

where P_i is the measurement of probe i and G is the interpolated bull gear profile.

[14] W. Kuehn, op. cit., pp. 10–12.

[15] W. Kuehn, op. cit., p. 12.

As a result of the bearing pad deflection, inaccuracies exist with either the measurement of the bearing film height and/or the measurement of the runner profile. The uncertainty exists in the film height and runner profile measurements because the deflection of the bar to which probes 1 through 5 are attached is unknown. If one assumes that the probe bar is attached in such a way that its deflection curve is exactly that of the pad as shown in Fig. 28, then the measurements taken by probes 1 through 5 represent the true film height. However, this results in inaccuracies because the distance between probes 1 through 5 and the line extended between the pad contact points of probes 6 and 7 is not the same for each probe as is assumed when computing the runner profile using Eq. (20). If one assumes that the probe bar is attached in such a way that it does not deflect at all as shown in Fig. 29, then the distance between probes 1 through 5 and the line extended between the pad contact points of probes 6 and 7 are the same for each probe, but probes 1 through 5 do not all measure the true film height. If the probe bar deflects differently than the bearing pad then there are inaccuracies in both the film height measurements and the runner profile measurements.

During construction, the hydrostatic bearing runner was installed such that the surface of the runner was flat in an unloaded state as intended by the bearing design. Because probes 1 through 5 are at the edge of the pad, they measure the profile of the runner in its deflected state. Hence, the current means of measuring the runner profile does not establish if the runner is flat in an unloaded state.

Station personnel have claimed that antenna shut downs have occurred in the past because oil contaminants have become stuck beneath the sensor probes. Since station personnel have found contaminant particles beneath the probes in the past it is clear that contaminant particles present in the hydrostatic bearing reservoir are another source of uncertainty when measuring the bearing film height and runner profile.

As the antenna rotates there is metal-to-metal rubbing contact between the tips of the probes measuring film height and the runner. Over time the tips of the probes and the runner surface will wear, resulting in uncertain measurement of the bearing film height and the runner profile.

The accurate determination of the runner profile is very dependent on knowing the profile of the bull with respect to an arbitrary plane perpendicular to gravity as evident from Eq. (20). As previously stated the bull gear profile is determined using a bar leveled with respect to gravity to measure the differences in bull gear elevation at 10-degree intervals. An electronic level is used to level the bar and an LVDT transducer is used to measure the difference in bull gear elevations at 10-degree intervals. There is some uncertainty in the measurement which is unknown. Because the bull gear profile at a point on the bull gear is determined by adding the elevation differences between a reference point A and point B where the bull gear profile height is desired, the error in the measurement of the bull gear profile is the sum of the measurement errors of all 10-degree intervals between point A and point B. Because there are 36 10-degree intervals, the uncertainty in the bull gear profile increases rapidly as one goes around the bull gear. Evidence of this is provided by station personnel at DSS 14 who claim that it is difficult to sum the elevation differences between all 36 intervals and obtain a sum within 254 μm (0.01 in.) of zero. Station personnel at DSS 14 have also indicated that it is impossible to obtain repeatability of any bull gear profile measurements if the antenna brakes are set during the measurement process. This indicates that the bull gear is not a constant reference point as it is currently treated for runner profile measurement and shimming purposes. Visible cracking of the antenna pedestal around the bull gear sole plates at DSS 14 provides further evidence supporting the claim that the bull gear profile is not constant. The movement of the bull gear at DSS 14 is expected to be a major source of runner profile measurement error. As of December 1992, a bull gear survey had not been performed at DSS 14 since February 1991, and since 1986, the data collected from a bull gear survey had not been entered into the computer program used to calculate the runner profile.

Inspection of the bull gear surface upon which measurements are taken by probe 9, which is used to reference the alidade frame to the bull gear, reveals that the top of the bull gear is a greased surface with many deep scratches and exposed to the atmosphere. Because the surface is exposed to the atmosphere, there is no guarantee that contaminants present on the bull gear do not affect the accuracy of the measurement of the position of the alidade frame with respect to the bull gear as measured by probe 9.

As the result of the numerous sources of measurement and computational errors presented above, there is uncertainty in just how accurately the hydrostatic bearing instrumentation group is able to measure bearing film height and runner profile. The inability to accurately measure the runner profile and film height can only create problems for the ongoing effort to maintain the 70-meter antenna runner flat in an unloaded state.

V. Conclusion

The program "A Computer Solution for Hydrostatic Bearings with Variable Film Thickness" originally used to design the 64-meter antenna hydrostatic bearing was modified in order to improve the ability of the program to accurately predict the film height profile between the hydrostatic bearing pad and the runner. The modified computer program is an improvement over the original because it considers pedestal deflections, pad deflections, and imperfections in the runner flatness when making predictions of the film height profile and oil pressure distribution. The results of several computer simulation runs were presented to show the sensitivity of the minimum bearing film height and recess pressures to oil temperature, oil type, recess flow rate, bearing load, pedestal deflection, pad deflection, and runner profile. This information can be used to assess the effects on bearing performance of any proposed additional pad loads or modifications to the hydrostatic bearing system. The computer analysis indicated that the minimum film height is significantly less than predicted during the 1960s' design analysis because pedestal and pad deflections were not considered during the original analysis. The analysis also revealed that a 6-K (10.8-deg-F) decrease in oil temperature from the normal operating temperature results in a 37.5-μm (0.0014-in.) increase in minimum film height, a 15.38-percent increase in pad load results in a 29.8-μm (0.0012-in.) decrease in minimum film height, and an 18.18-percent decrease in recess flow results in a 12.9-μm (0.0005-in.) decrease in minimum film height. The effect on bearing performance of the runner profile at DSS 14 as measured by the hydrostatic bearing instrumentation group was presented. The current value of using the modified hydrostatic bearing computer program to evaluate the effect of actual runner profiles, such as the one from DSS 14 used in this study, is questionable because the uncertainty of the runner profile and film height measurements made by the hydrostatic bearing instrumentation group is not well defined for the reasons stated in this article. The accuracy of the measurements made by the hydrostatic bearing instrumentation group should be well defined since these are the measurements upon which the hydrostatic bearing runner is shimmed and low film height alarms are made.

Reference

[1] J. Halling, *Principles of Tribology*, London, Great Britain: Macmillan Education LTD, 1978.

Appendix

Glossary

a	constant
a_i	constant
b	constant
$b(x,y)$	runner profile under pad coordinates (x,y) positive up
$d_o(x,y)$	Green's function at pad coordinates (x,y)
$d_o^*(x,y)$	Green's function at pad coordinates (x,y)
$d_u(x,y)$	Green's function at pad coordinates (x,y)
$e(x,y)$	pedestal deflection positive up at coordinates (x,y)
E	modulus of elasticity
$g(x,y)$	pad deflection positive up at pad coordinates (x,y)
G	bull gear profile with respect to a reference plane perpendicular to gravity
h	film height
$h_{\min}$	minimum film height
$h(x,y)$	film height at pad coordinates (x,y)
m	constant
p	pressure
Δp	differential pressure across the pump
P_{avg}	average pressure
P_i	pressure in recess number i, reading of probe number i, average pressure of area number i
P_o	pressure
P_o^*	pressure
q_x	oil flow rate at a point under the pad in the x direction through an area of height h and width dy
q_y	oil flow rate at a point under the pad in the y direction through an area of height h and width dx
Q	pump flow rate
Q_i	oil flow into recess number i
r_d	radius where the deflection is desired
r_L	radius at which a load is applied
S	pump rotational speed in rpm
T	absolute temperature, vertical distance between probes 1 through 5 and the line extended between the pad contact point of probes 6 and 7
W	load on the bearing pad
W_x	moment on the bearing pad about the x-axis
W_y	moment on the bearing pad about the y-axis
x	Cartesian coordinate

x	Cartesian coordinate
X	vertical distance between the top of the bearing pad and a reference point on the alidade frame
y	Cartesian coordinate
Y	vertical distance between the top of the bull gear and a reference point on the alidade frame
Z	runner profile from the reference plane
Z_i	runner profile from the reference plane as measured by probe number i
η	dummy variable
θ_d	angle between the applied load and the point where the deflection is desired
μ	absolute viscosity
ν	kinematic viscosity, Poisson's ratio
ξ	dummy variable
ρ	oil density
ϕ_x	pad tilt angle about the x-axis
ϕ_y	pad tilt angle about the y-axis

Table 1. Recess pressures and minimum film height when different oil flow rates are provided to each recess. Each computer simulation was performed using ISO 150 oil at a temperature of 308 K and a pad load of 1.3×10^7 newtons. Pedestal and pad deflections were considered with the pad centered at 135 deg trough azimuth over the runner profile shown in Fig. 5.

Pump flow rate, ml/sec						Recess pressure, MPa						h_{min}, μm
Q_1	Q_2	Q_3	Q_4	Q_5	Q_6	P_1	P_2	P_3	P_4	P_5	P_6	
550	550	550	550	550	550	9.88	10.06	9.96	10.24	10.03	10.33	151.6
350	550	550	550	550	550	9.23	10.38	9.89	10.37	10.21	10.00	132.6
550	350	550	550	550	550	10.06	9.75	10.16	10.28	10.02	10.37	143.5
650	550	550	550	550	550	10.03	10.01	9.96	10.18	10.03	10.37	153.0
550	650	550	550	550	550	9.63	10.40	9.72	10.09	10.22	10.17	154.9
350	550	650	350	550	650	9.53	10.33	9.79	9.88	10.32	10.17	119.1

Table 2. Effect of pedestal and pad deflections on recess pressures and minimum film height. Each computer simulation was performed using ISO 150 oil at a temperature of 308 K, a pad load of 1.3×10^7 newtons, recess flows of 550 ml/sec, and a flat runner profile.

Pedestal deflection	Pad deflection	Recess pressure, MPa						h_{min}, μm
		P_1	P_2	P_3	P_4	P_5	P_6	
No	No	9.96	11.49	9.96	9.96	11.49	9.96	273.4
No	Yes	7.13	15.02	7.12	7.13	15.03	7.11	199.3
Yes	No	10.65	9.27	11.00	11.01	9.42	11.13	102.68
Yes	Yes	10.14	10.03	10.23	10.29	10.01	10.38	158.72

Table 3. A comparison of the recess pressures and minimum film height when a flat runner is used and when the runner profile shown in Fig. 5 is used with the pad centered at 135 deg trough azimuth. Each computer simulation was performed using ISO 150 oil at a temperature of 308 K, a pad load of 1.3×10^7 newtons, and recess flows of 550 ml/sec. Pedestal and pad deflections were considered.

Flat runner	Recess pressure, MPa						h_{min}, μm
	P_1	P_2	P_3	P_4	P_5	P_6	
Yes	10.14	10.03	10.23	10.29	10.01	10.38	158.72
No	9.88	10.06	9.96	10.24	10.03	10.33	151.6
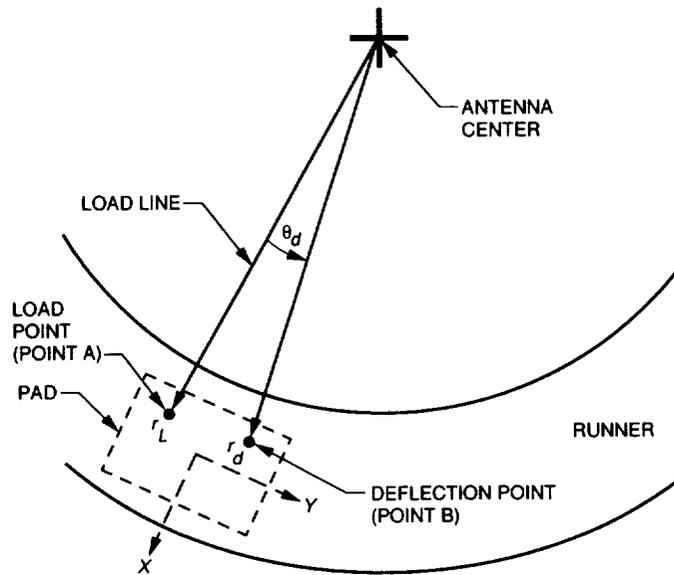
Fig. 1. Geometry and coordinate system of the antenna pedestal
and pad as viewed from the top.
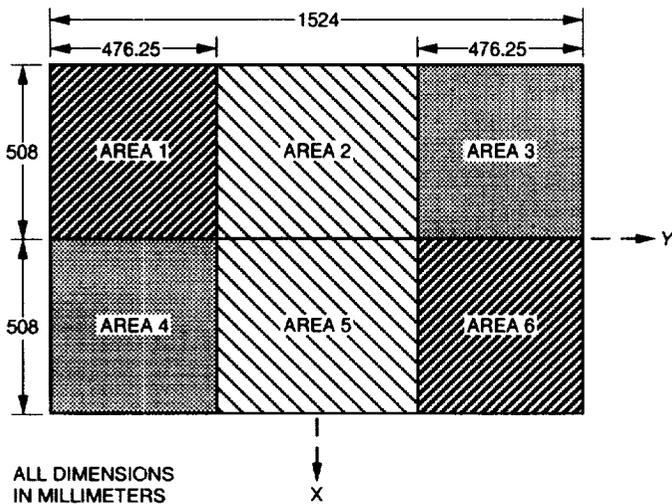
Fig. 2. Component pressure distributions used to compute the
deflection of the hydrostatic bearing pad.
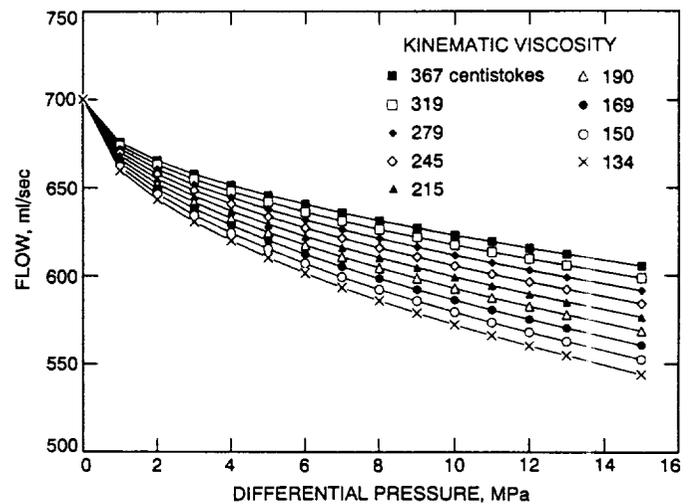
Fig. 3. Output flow rate of an unworn De Laval Turbine, Inc., IMO
B12-LBSX-118 pump operating at 1750 rev/min as a function of the
differential pressure across the pump and the kinematic viscosity
of the oil.

ALL DIMENSIONS IN MILLIMETERS
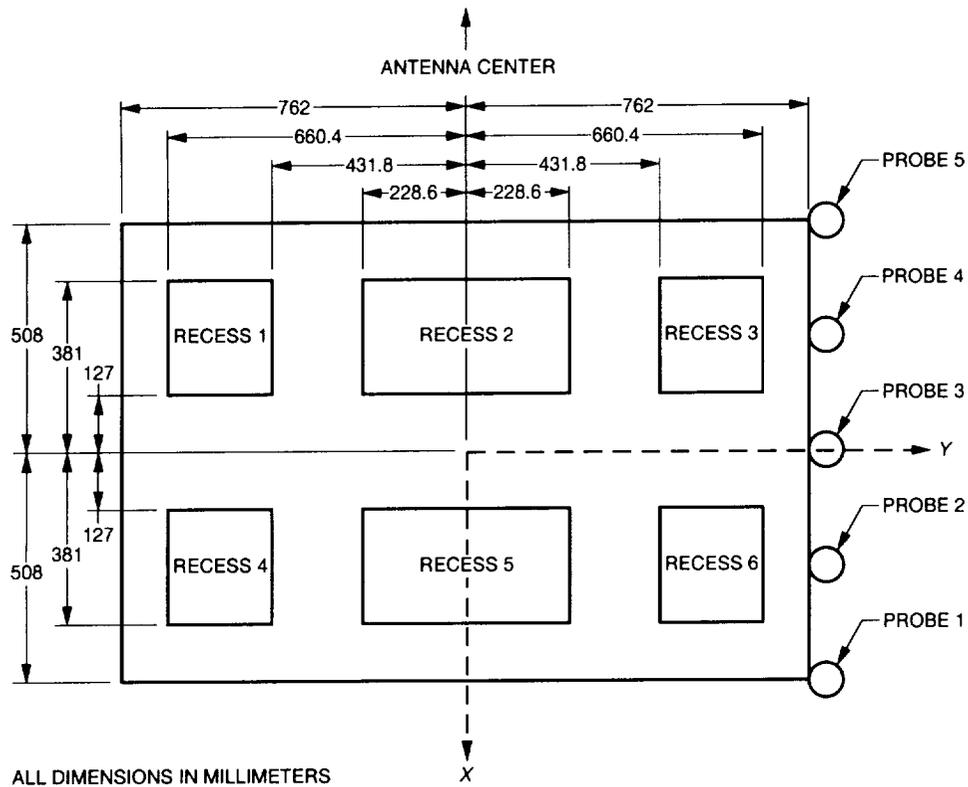
Fig. 4. Geometry and coordinate system of the DSN 70-meter antenna hydrostatic bearing pad number 3 as viewed from the top.
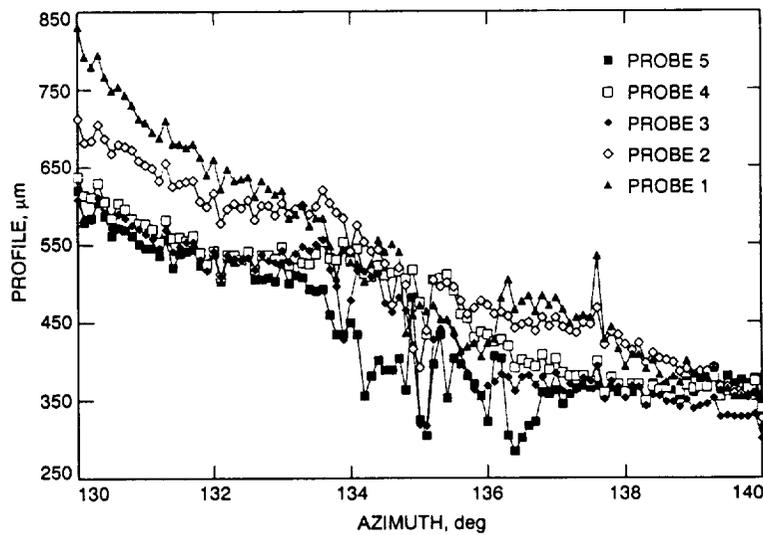
Fig. 5. DSS-14 hydrostatic bearing runner profile data collected on October 16, 1992, between 130 deg and 140 deg trough azimuth.
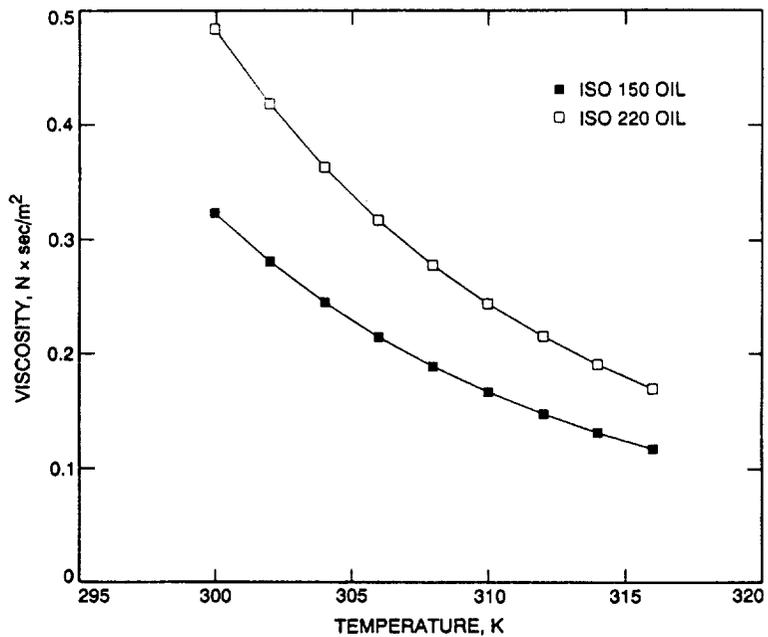
Fig. 6. Absolute viscosity of ISO 150 oil and ISO 220 oil as a function of temperature.
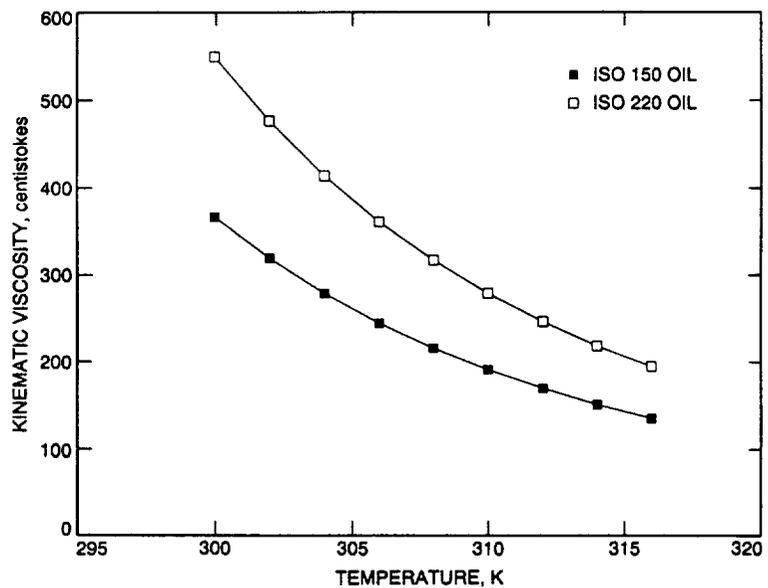
Fig. 7. Kinematic viscosity of ISO 150 oil and ISO 220 oil as a function of oil temperature.

162
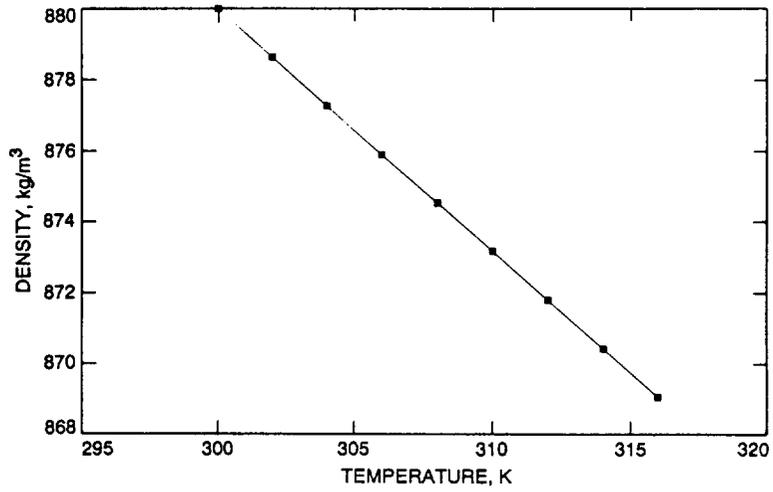
Fig. 8. Density of ISO 150 and ISO 220 oil as a function of oil temperature.
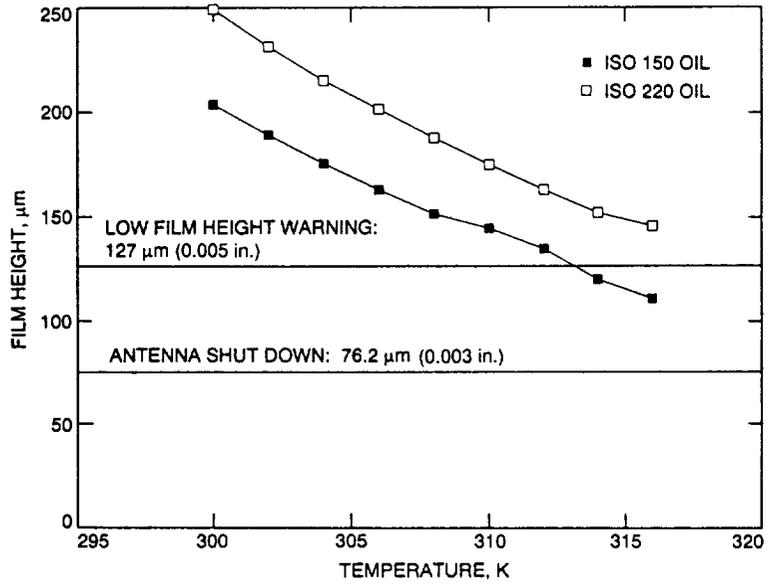
Fig. 9. Minimum film height as a function of temperature for ISO 150 oil and ISO 220 oil. All of the hydrostatic bearing simulations used to produce this graph were performed using a pad load of 1.3×10^7 newtons, recess flows of 550 ml/sec, and the runner profile shown in Fig. 5 with the pad centered at 135 deg trough azimuth. Pedestal and pad deflections were considered during each simulation.
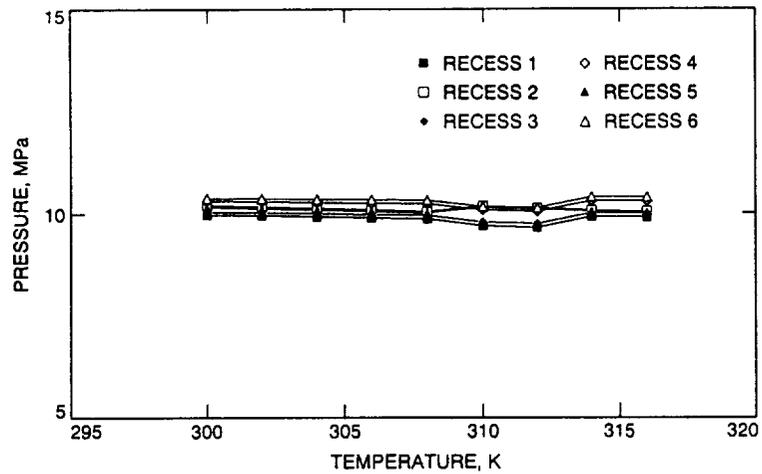
Fig. 10. Recess pressures as a function of temperature when using ISO 150 oil. All of the hydrostatic bearing simulations used to produce this graph were performed using a pad load of 1.3×10^7 newtons, recess flows of 550 ml/sec, and the runner profile shown in Fig. 5 with the pad centered at 135 degrees trough azimuth. Pedestal and pad deflections were considered during each simulation.
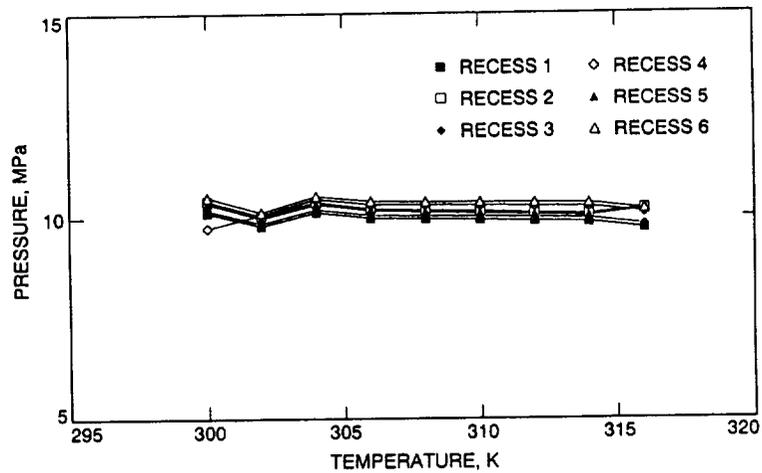

Fig. 11. Recess pressures as a function of temperature when using ISO 220 oil. All of the hydrostatic bearing simulations used to produce this graph were performed using a pad load of 1.3×10^7 newtons, recess flows of 550 ml/sec, and the runner profile shown in Fig. 5 with the pad centered at 135 degrees trough azimuth. Pedestal and pad deflections were considered during each simulation.
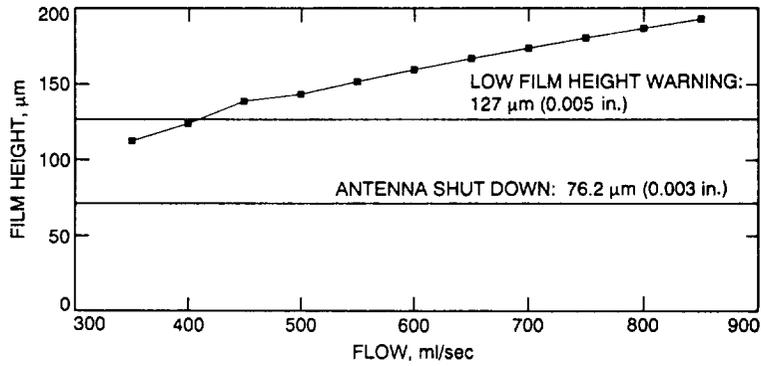
Fig. 12. Minimum film height as a function of recess flow rate when using ISO 150 oil. All of the hydrostatic bearing simulations used to produce this graph were performed using a pad load of 1.3×10^7 newtons, an oil temperature of 308 K, and the runner profile shown in Fig. 5 with the pad centered at 135 degrees trough azimuth. Pedestal and pad deflections were considered during each simulation.
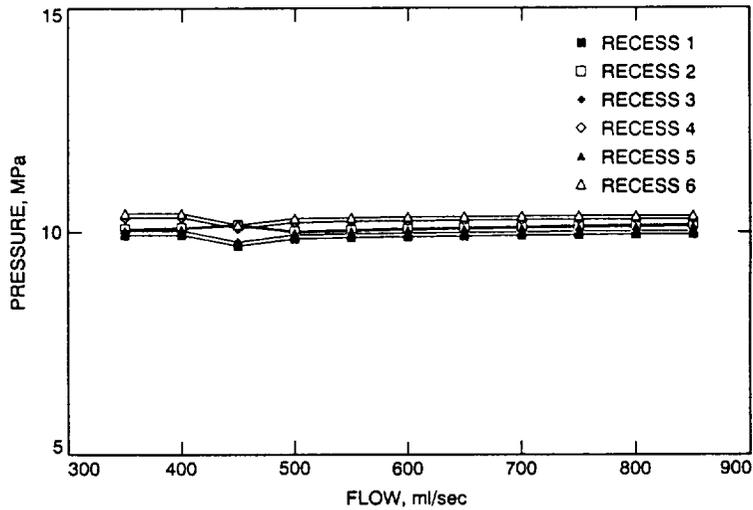
Fig. 13. Recess pressures as a function of recess flow rate when using ISO 150 oil. All of the hydrostatic bearing simulations used to produce this graph were performed using a pad load of 1.3×10^7 newtons, an oil temperature of 308 K, and the runner profile shown in Fig. 5 with the pad centered at 135 degrees trough azimuth. Pedestal and pad deflections were considered during each simulation.
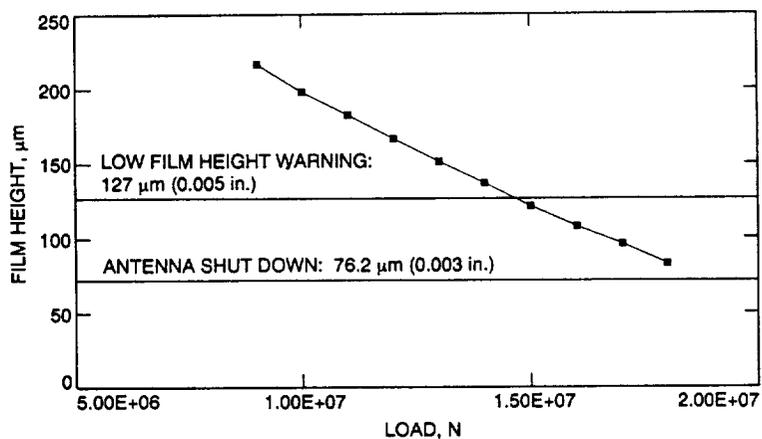
Fig. 14. Minimum film height as a function of pad load when using ISO 150 oil. All of the hydrostatic bearing simulations used to produce this graph were performed using an oil temperature of 308 K, recess flows of 550 ml/sec, and the runner profile shown in Fig. 5 with the pad centered at 135 degrees trough azimuth. Pedestal and pad deflections were considered during each simulation.
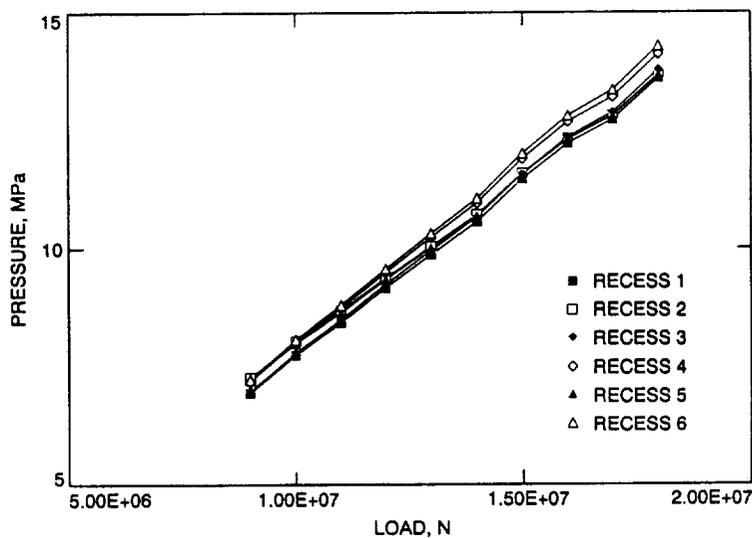
Fig. 15. Recess pressures as a function of pad load when using ISO 150 oil. All of the hydrostatic bearing simulations used to produce this graph were performed using an oil temperature of 308 K, recess flows of 550 ml/sec, and the runner profile shown in Fig. 5 with the pad centered at 135 degrees trough azimuth. Pedestal and pad deflections were considered during each simulation.
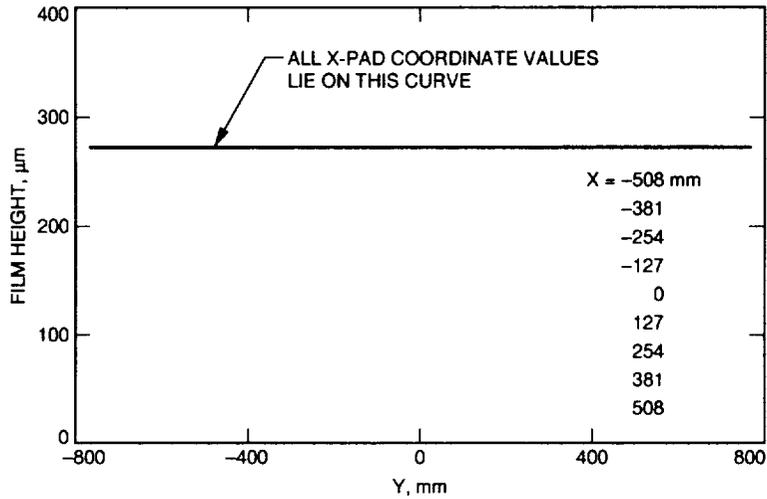
Fig. 16. Oil film height profile as a function of the Y-pad coordinate when the pedestal and pad do not deflect. The computer simulation was performed using ISO 150 oil at a temperature of 308 K, a pad load of 1.3×10^7 newtons, recess flows of 550 ml/sec, and a flat runner profile.
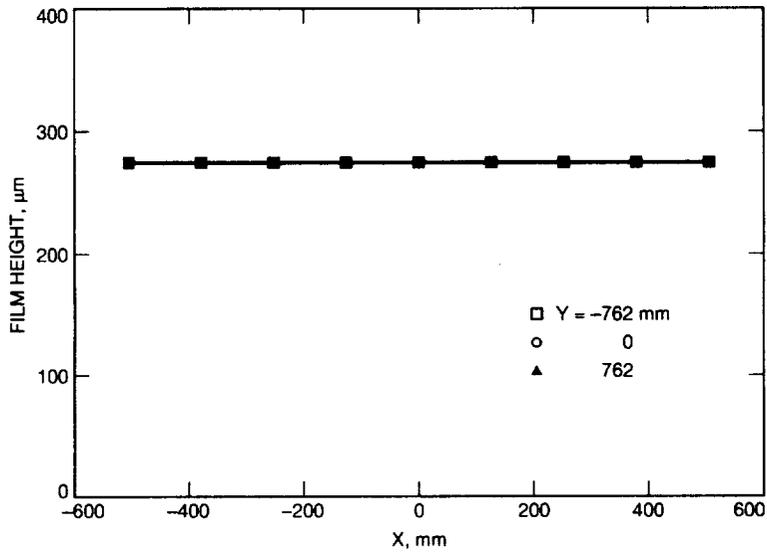

Fig. 17. Oil film height profile as a function of the X-pad coordinate when the pedestal and pad do not deflect. The computer simulation was performed using ISO 150 oil at a temperature of 308 K, a pad load of 1.3×10^7 newtons, recess flows of 550 ml/sec, and a flat runner profile.
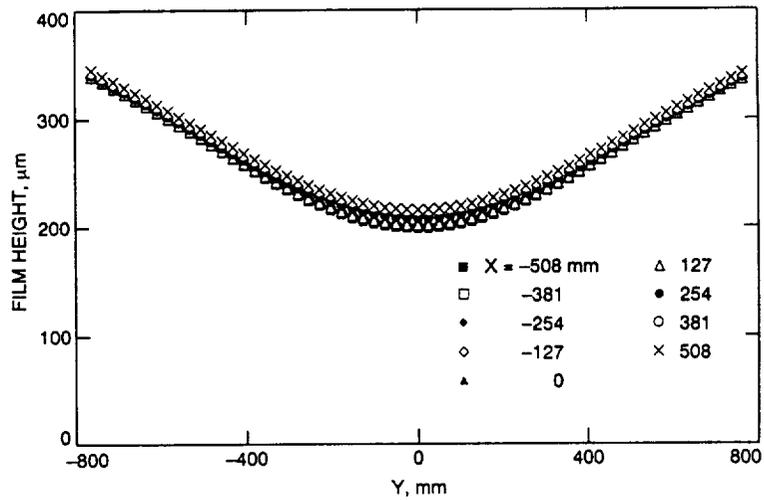
Fig. 18. Oil film height profile as a function of the Y-pad coordinate when the pedestal does not deflect and the pad deflects. The computer simulation was performed using ISO 150 oil at a temperature of 308 K, a pad load of 1.3×10^7 newtons, recess flows of 550 ml/sec, and a flat runner profile.
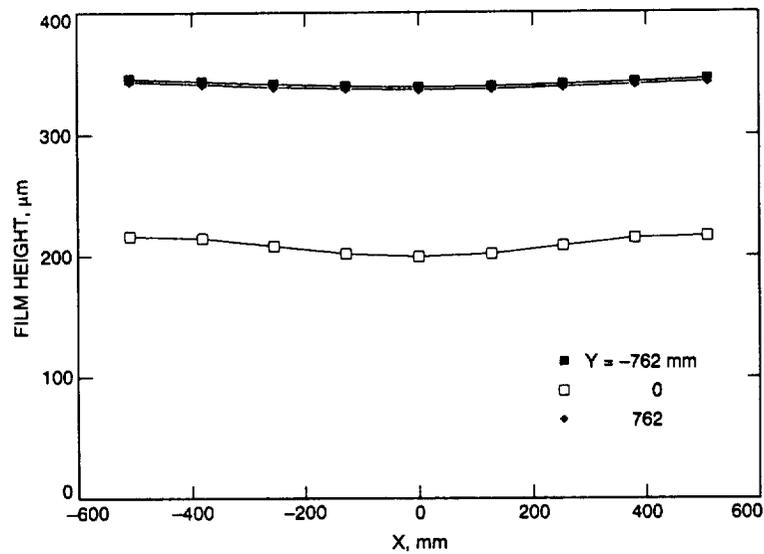
Fig. 19. Oil film height profile as a function of the X-pad coordinate when the pedestal does not deflect and the pad deflects. The computer simulation was performed using ISO 150 oil at a temperature of 308 K, a pad load of 1.3×10^7 newtons, recess flows of 550 ml/sec, and a flat runner profile.
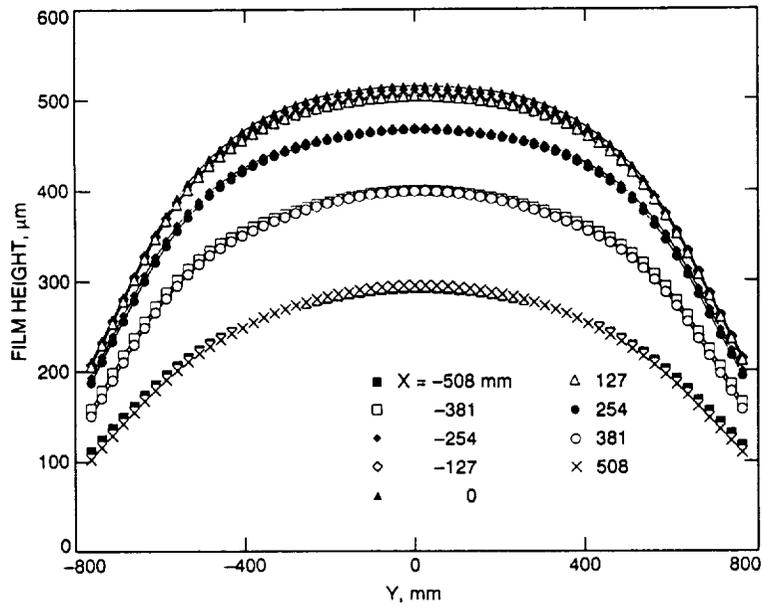
Fig. 20. Oil film height profile as a function of the Y-pad coordinate when the pedestal deflects and the pad does not deflect. The computer simulation was performed using ISO 150 oil at a temperature of 308 K, a pad load of 1.3 × 10^7 newtons, recess flows of 550 ml/sec, and a flat runner profile.
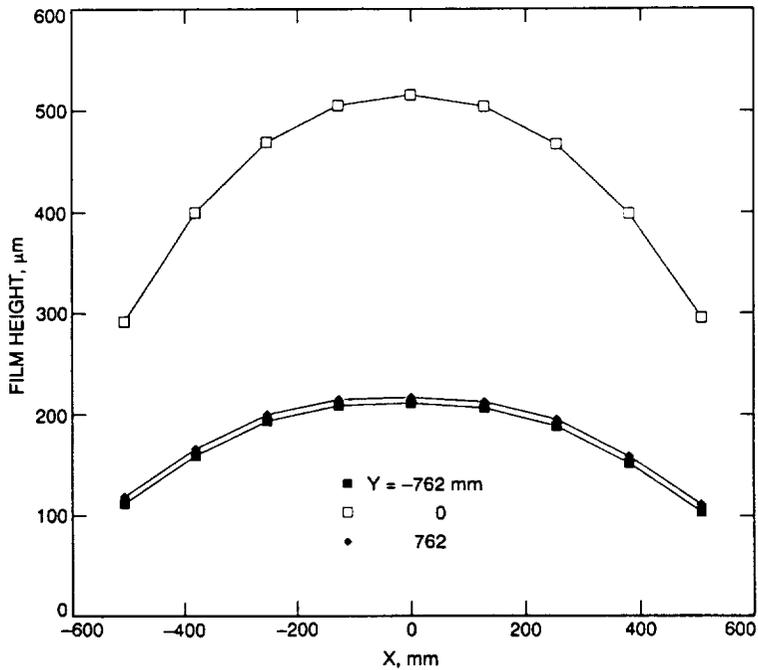

Fig. 21. Oil film height profile as a function of the X-pad coordinate when the pedestal deflects and the pad does not deflect. The computer simulation was performed using ISO 150 oil at a temperature of 308 K, a pad load of 1.3 × 10^7 newtons, recess flows of 550 ml/sec, and a flat runner profile.
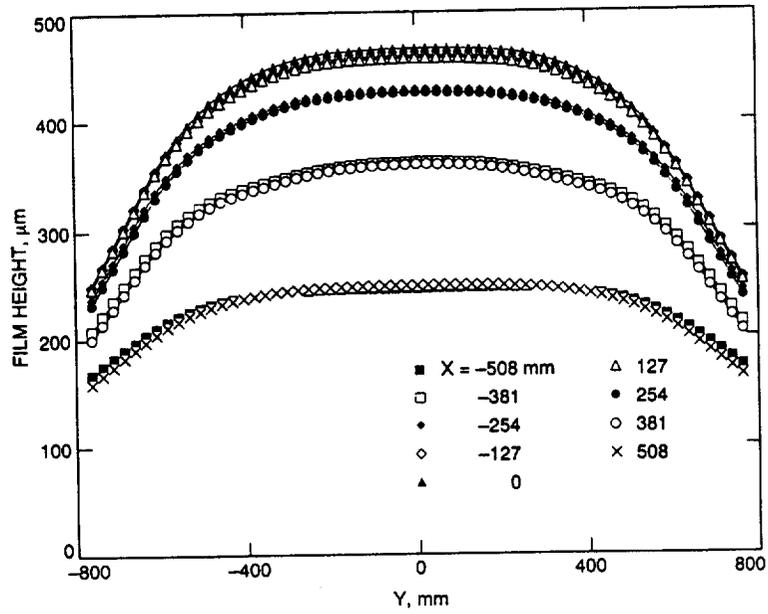
Fig. 22. Oil film height profile as a function of the Y-pad coordinate when the pedestal and the pad deflect. The computer simulation was performed using ISO 150 oil at a temperature of 308 K, a pad load of 1.3×10^7 newtons, recess flows of 550 ml/sec, and a flat runner profile.
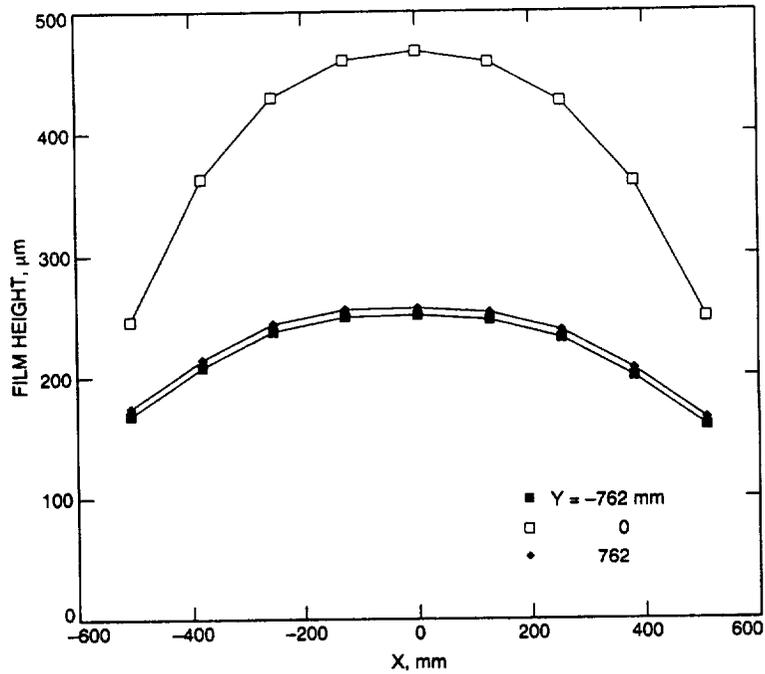

Fig. 23. Oil film height profile as a function of the X-pad coordinate when the pedestal and the pad deflect. The computer simulation was performed using ISO 150 oil at a temperature of 308 K, a pad load of 1.3×10^7 newtons, recess flows of 550 ml/sec, and a flat runner profile.
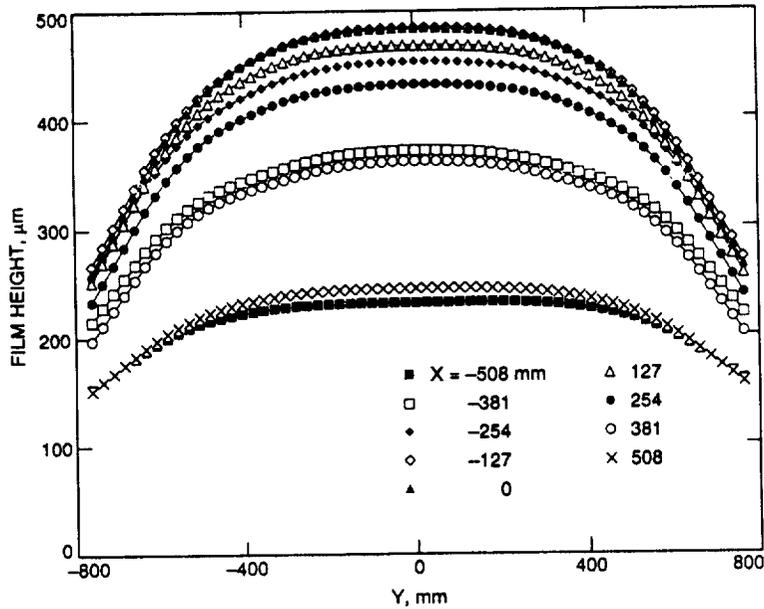
Fig. 24. Oil film height profile as a function of the Y-pad coordinate when the pedestal and the pad deflect. The computer simulation was performed using ISO 150 oil at a temperature of 308 K, a pad load of 1.3 × 10^7 newtons, recess flows of 550 ml/sec, and the runner profile shown in Fig. 5 with the pad centered at 135 degrees trough azimuth.
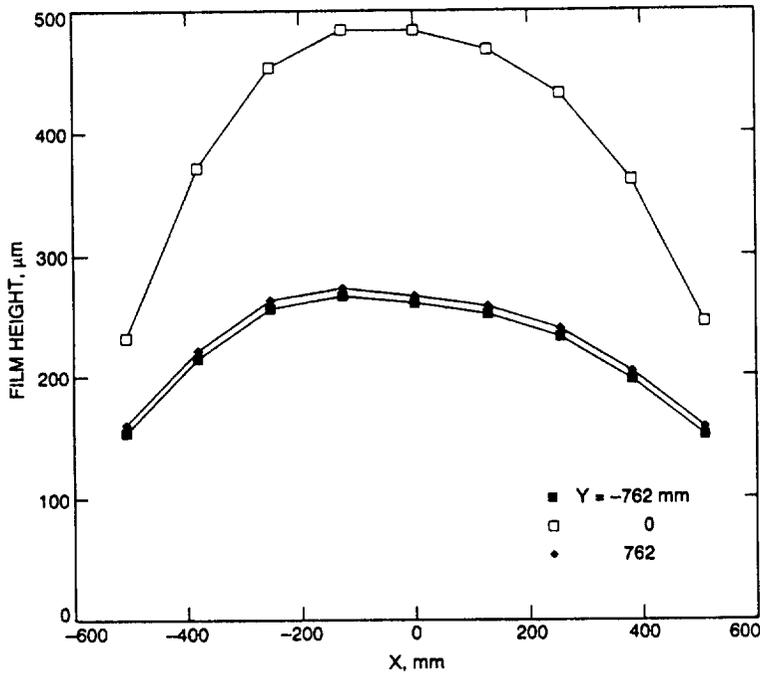
Fig. 25. Oil film height profile as a function of the X-pad coordinate when the pedestal and the pad deflect. The computer simulation was performed using ISO 150 oil at a temperature of 308 K, a pad load of 1.3 × 10^7 newtons, recess flows of 550 ml/sec, and the runner profile shown in Fig. 5 with the pad centered at 135 degrees trough azimuth.

171

C-3
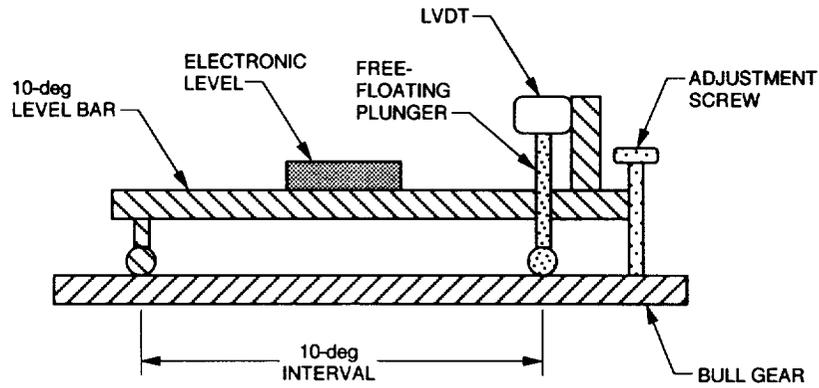
Fig. 26. Ten-degree level bar used to measure the bull gear profile.
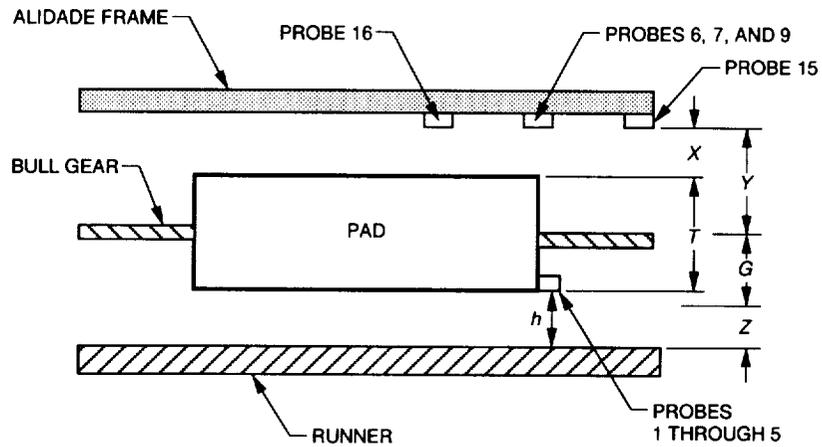
Fig. 27. Hydrostatic bearing pad, runner, bull gear, and alidade frame viewed radially while facing toward the antenna center.
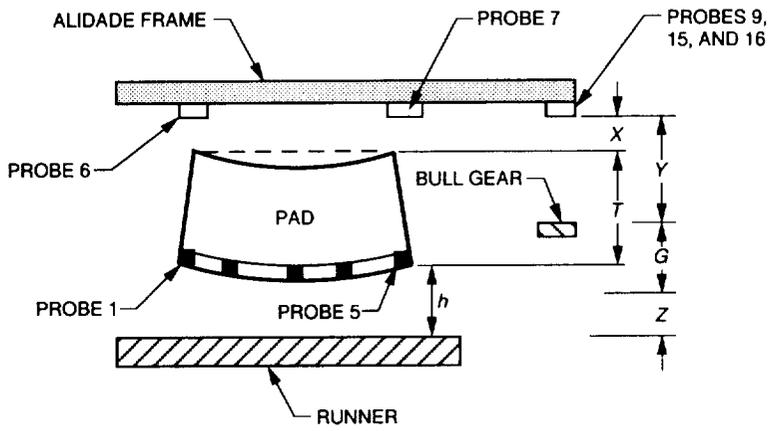
Fig. 28. Hydrostatic bearing pad, runner, bull gear, and alidade frame viewed tangentially while facing toward the probe bar on pad 3. The probe bar is assumed to deflect with the pad.
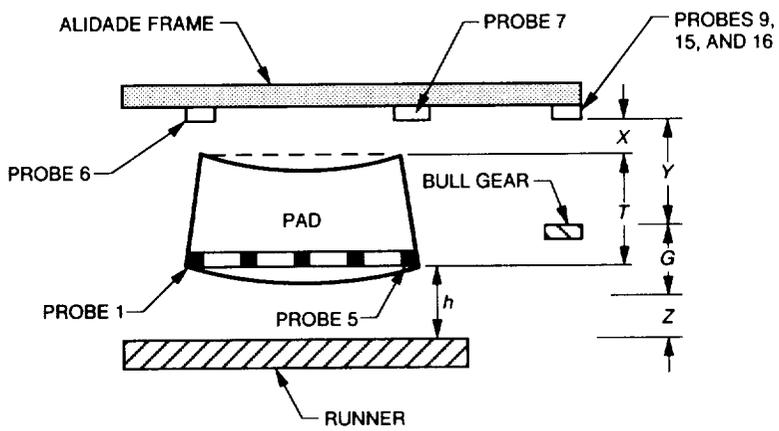

Fig. 29. Hydrostatic bearing pad, runner, bull gear, and alidade frame viewed tangentially while facing toward the probe bar on pad 3. The probe bar is assumed not to deflect.